CFRP SHEAR STRENGTHENING OF REINFORCED CONCRETE T-BEAMS WITH CORRODED SHEAR LINKS

Shunde Qin[1]; Samir Dirar[2]; Jian Yang[3]; Andrew H. C. Chan[4]; and Mohammed Elshafie[5]

ABSTRACT

This paper investigates the structural behavior of un-corroded as well as corroded reinforced concrete (RC) T-beams strengthened in shear with either externally bonded (EB) carbon fiber-reinforced polymer (CFRP) sheets or embedded CFRP rods. Nine tests were carried out on RC T-beams having an effective depth of 295 mm and a shear span to effective depth ratio of 3.05. The investigated parameters are the shear link corrosion level (un-corroded, 7% corroded, or 12% corroded) and type of CFRP strengthening system (EB CFRP sheets or embedded CFRP rods). The unstrengthened beams with shear link corrosion levels of 7% and 12% had shear strengths that were 11% and 14% respectively less than the shear strength of the un-corroded unstrengthened beam. Both the embedded CFRP rods and EB CFRP sheets were effective in enhancing the shear strength of tested beams but the effectiveness of both strengthening systems decreased with increasing shear link corrosion level. The shear strength enhancement provided by the embedded CFRP rods and EB CFRP sheets decreased from 19% and 15% respectively to 12% and 11% respectively with the increase in shear link corrosion level from 7% to 12%. Corrosion of the shear links did not have a significant effect

[1] Ph. D. Candidate, School of Civil Engineering, University of Birmingham, Edgbaston, Birmingham, B15 2TT, United Kingdom, E-mail: sxq482@bham.ac.uk
[2] Lecturer in Structural Engineering, School of Civil Engineering, University of Birmingham, Edgbaston, Birmingham, B15 2TT United Kingdom (corresponding author), E-mail: s.m.o.h.dirar@bham.ac.uk
[3] Lecturer in Structural Engineering, School of Civil Engineering, University of Birmingham, Edgbaston, Birmingham, B15 2TT, United Kingdom, E-mail: j.yang.3@bham.ac.uk
[4] Professor, School of Science, Information Technology and Engineering (Ballarat), Federation University Australia, Victoria 3350, Australia, E-mail: a.chan@federation.edu.au
[5] Lecturer in Construction Engineering, Department of Engineering, University of Cambridge, Cambridge, CB2 1PZ, United Kingdom, E-mail: me254@cam.ac.uk

on the beam stiffness. Premature debonding limited the effectiveness of the EB CFRP sheets whereas the embedded CFRP rods did not exhibit signs of debonding and therefore showed higher effectiveness.

CE Database subject headings: Beams; Corrosion; Epoxy; Fiber reinforced polymer; Rehabilitation; Reinforced concrete; Rods; Shear strength; Sheets

INTRODUCTION

Annually, large amounts of money are spent on repairing corrosion-damaged reinforced concrete (RC) structures. In the United Kingdom (UK) alone, it has been estimated that the cost of repairing corrosion-damaged RC bridges is about £616.5 million (Broomfield, 2007). In the United States, the situation is even worse as the annual estimated direct cost of replacing or repairing corrosion-damaged bridges is $8.3 billion (Koch et al., 2001). Other countries in North America and Europe are faced with the same challenge, so emphasizing the global significance of the issue.

The use of de-icing salts in cold regions and/or windborne salts in coastal/marine environments are the main causes of chloride contamination of concrete (El-Maaddawy and Chekfeh, 2013). Chlorides break down the protective passive layer of iron oxides around the internal steel reinforcement and thereby facilitate the corrosion process. The volume of the corrosion products, which is larger than that of the steel consumed in the corrosion process, stresses the surrounding concrete and initiates cracking and spalling of the concrete cover (El Maaddawy and Soudki, 2007).

Internal steel shear links are susceptible to corrosion due to their proximity to the outer surfaces of concrete members. Corrosion of the internal steel shear links can have a detrimental impact on the shear strength of RC beams, and may lead to sudden and catastrophic brittle failure (Xia et al., 2011). There is thus scope for safe, practical, and durable shear strengthening methods.

In the last two decades, the use of fiber-reinforced polymer (FRP) reinforcement for retrofitting RC structures has become a field of much research interest. FRPs have several advantages over classic strengthening techniques, such as design flexibility, ease of use, and corrosion resistance. Methods for shear strengthening of RC beams using FRP composites include externally bonded (EB) sheets (Dirar et al., 2012) or plates (Mofidi et al., 2014), near-surface mounted (NSM) bars (Rahal and Rumaih, 2011), prestressed carbon fiber reinforced polymer (CFRP) straps (Dirar et al., 2013) and embedded CFRP rods (Valerio et al. 2009; Mofidi et al. 2012a). Compared with the EB and NSM shear strengthening methods, the deep embedment (DE) technique – also known as the embedded through section technique – (Valerio and Ibell 2003; Valerio et al. 2009; Mofidi et al. 2012a) offers better bond performance between the concrete and the FRP reinforcement (Chaallal et al., 2011).

A careful review of the published literature reveals that research studies investigating the shear behavior of RC beams strengthened using the DE technique is scarce. Moreover, very few studies have considered the behavior of CFRP shear-strengthened RC T-beams with corroded shear links (El-Maaddawy and Chekfeh, 2013). Furthermore, to date, there are no research studies comparing the effectiveness of the EB and embedded CFRP shear strengthening systems in the context of RC T-beams with corroded shear reinforcement.

This paper presents the results of nine tests on un-strengthened as well as CFRP-strengthened RC T-beams with either un-corroded or corroded steel shear links. EB CFRP sheets or embedded CFRP rods are used as shear strengthening systems in this study.

RESEARCH SIGNIFICANCE

The strength enhancement of corrosion-damaged concrete infrastructure is an application of considerable economic importance, particularly in the case of bridges. This investigation examines the effectiveness of two CFRP systems for shear strengthening of concrete structures with corroded shear links. The effect of shear link corrosion level on the shear force capacity and shear strength enhancement provided by the CFRP systems has been elucidated. As a matter of interest to owners, managers, and designers of concrete infrastructure, the investigated CFRP systems show potential for enhancing the shear strength of corrosion-damaged concrete structures.

EXPERIMENTAL INVESTIGATION

The experimental program comprised 9 RC T-beams categorized into three groups as summarized in Table 1. Each group included three beams with a targeted shear link corrosion level in a given beam of 0% (i.e. un-corroded), 7%, or 15%. Different durations of exposure to corrosion and applied current densities were used, as reported in Table 1, to corrode the shear links. Further details about the accelerated corrosion process are given below.

Each beam had a two-part designation consisting of an alphabetical letter (N, R, or S) followed by a number (00, 07, or 12). The alphabetical letter indicates that a beam was unstrengthened (N), strengthened with embedded CFRP rods (R), or strengthened with EB CFRP sheets (S). The number refers to the actual shear link corrosion level in a given beam. Hence, the designation N00 refers to an unstrengthened un-corroded beam whereas the designation R12 refers to a beam with an actual shear link corrosion level of 12% and strengthened with embedded CFRP rods.

All beams were 2.7 m long and had T-shaped cross-sections (see Figure 1) in order to simulate existing slab-on-beam RC structures. The web width (b_w), flange width, and flange thickness were 125 mm, 260 mm, and 100 mm respectively. The beams had a shear span to effective depth ratio of 3.05 and an effective depth (d) of 295 mm. The beams were designed to fail in shear and had a significant difference between their unstrengthened shear force capacity and their flexural capacity so as to provide a sufficient range over which the level of shear strength enhancement could be measured.

All beams were reinforced with steel flexural and shear reinforcement. The longitudinal steel reinforcement consisted of three 20 mm compression bars and four 25 mm tension bars. The compression reinforcement was anchored with a 230 mm × 50 mm × 25 mm welded steel plate at each end. The tension reinforcement was anchored with a 100 mm × 100 mm × 25 mm welded steel plate at each end so as to prevent bond failure. The internal steel shear links were 8 mm in diameter. The spacing of the steel shear links was 275 mm centre-to-centre within the test span and 100 mm centre-to-centre within the non-test span (see Figure 2a). The steel shear link spacing of 275 mm (0.93d) is representative of earlier design practice in the UK which allowed shear link spacing of up to the effective member depth (Concrete Society, 2009).

The CFRP shear strengthening scheme consisted of either one layer of continuous U-shaped EB CFRP sheets or 10 mm sand-coated embedded CFRP rods spaced at 275 mm centre-to-centre. The CFRP rod spacing was chosen in such a way that the shear strength enhancement provided by the DE bars would at least counteract the shear strength reduction due to the higher shear link corrosion level. The bottom corners of the beams strengthened with the EB CFRP sheets were rounded along the test span to avoid stress concentrations in the EB CFRP reinforcement.

The beams were tested in a three-point bending configuration as shown in Figure 2. The centreline of each support was 250 mm from the corresponding beam end. The centre-to-centre distance between the support at the end of the test span and the hydraulic jack was 900 mm. Steel plates, 200 mm wide by 25 mm thick, were used as supporting plates whereas a 200 mm wide by 20 mm thick steel plate was used as a loading plate.

Materials

The beams were cast one at a time using the same concrete mixture proportions (cement: water: aggregate: sand = 1: 0.65: 2: 3) and a maximum aggregate size of 10 mm. In order to create a chloride concrete environment, 3% calcium chloride by mass of the cement was added to the concrete mixtures used for casting the corroded beams.

The values of the cube compressive strength, cylinder split tensile strength, and flexural strength, as obtained on testing day (i.e. either 28 days after casting for the un-corroded beams or after the accelerated corrosion process for the corroded beams), are summarised in Table 2. The targeted cube compressive strength (f_{cu}) was 30 MPa. However, due to unintended quality control issues, there were differences between the targeted and actual cube compressive strength values (see Table 2). In order to avoid such an unfortunate situation, it is recommended that, where possible, all beams be cast at the same time using the same concrete batch. This should at least ensure that all beans have comparable, if not similar, concrete strength values.

Tensile tests were carried out on the steel reinforcement bars to quantify their mechanical properties. The average test results for the strength and stiffness properties of the steel reinforcement are summarised in Table 3. The average values reported in Table 3 were based on three tested samples per bar. The standard deviation values for the strength and stiffness properties of the steel reinforcement were negligible.

The CFRP sheets used to repair the T-beams were unidirectional woven carbon fiber fabrics. They were used in conjunction with a two-component epoxy laminating resin to provide a composite strengthening system. The thickness, tensile strength, ultimate strain, and elastic modulus of the composite system as provided by the manufacturer are 1 mm, 986 MPa, 1%, and 95.8 GPa respectively.

The 10 mm sand-coated CFRP rods had a tensile strength, elastic modulus, and ultimate strain of 2172 MPa, 124 GPa, and 1.75% respectively. A commercially available high-viscosity epoxy resin was used for anchoring the embedded rods. As specified by the manufacturer, it had a bond strength, compressive strength, compressive modulus, tensile strength, and elongation at failure of 12.4 MPa, 82.7 MPa, 1493 MPa, 43.5 MPa, and 2% respectively.

Accelerated corrosion process

Figure 3 shows a schematic of the accelerated corrosion setup. Apart from the shear links within a test span, the internal steel flexural and shear reinforcement in the corroded beams together with the end plates were coated with aluminium pigmented epoxy to provide corrosion protection.

After concrete casting and a 28-day curing period, a test span was encircled with a stainless steel sheet and placed within a plastic tank containing 3% sodium chloride (NaCl) solution. The NaCl solution level was maintained at just above the top surface of the stainless steel sheet. The stainless steel sheet was connected to the cathode of a direct current (DC) power supply unit. The shear links in the test span of R12 were connected to each other and then to one of the positive terminals of the DC power supply unit. The shear links in the test spans of the remaining beams were each connected to the positive terminals of the DC power supply unit. The same DC power supply unit, which had twelve individually controllable positive terminals, was used for all beams.

Three current density values; namely 140, 185, and 200 $\mu A/cm^2$; were used as detailed in Table 1 to corrode the steel shear links. These current density levels, which are comparable with the current density value of 160 μA/cm^2 used by El-Maaddawy and Chekfeh (2013), were based on the findings of El-Maaddawy and Soudki (2003) who indicated that a current density higher than 200 μA/cm^2 would result in exaggerated concrete strains and crack widths.

Corrosion level

The targeted corrosion levels of 7% and 15% were chosen to represent medium and high corrosion levels respectively. The 15% corrosion level was selected based on the findings of Almusallam (2001) who showed that corrosion levels of about 12% resulted in significant reductions in the yield and ultimate stresses and strains of steel reinforcing bars.

The theoretical time required to achieve such corrosion levels was calculated using Faraday's law. The actual corrosion levels were determined after testing using gravimetric mass loss analysis. Before casting the corroded beams, the original mass and length of the shear links to be corroded were recorded. After testing, the corroded shear links were extracted from the concrete and the recommendations of ASTM G1-03 (2011) were used to calculate the actual corrosion level.

Installation of CFRP sheets

Before installing the CFRP sheets, the web of a test span was roughened with a grinder. The rounded corners at the soffit (see Figure 1) were further smoothened to reduce stress concentrations. The prepared surface was then cleaned with a wire brush and compressed air. It was also ensured that the surface was dry and free from any oil or greasy substances.

Upon completion of the surface preparation process, the two-component epoxy resin was used to impregnate the CFRP sheets. A uniform layer of epoxy was then applied to the web at a thickness of approximately 1 mm. The epoxy was also used to fill any pores on the concrete surface. A layer of the epoxy-impregnated CFRP sheets was then pressed gently onto the web. A plastic trowel was used to remove air bubbles beneath the CFRP sheets. Eventually, a final layer of epoxy was applied to protect the CFRP sheets. The composite material was then left to cure at room temperature.

Installation of CFRP rods

In order to install the CFRP rods, 15 mm diameter vertical holes were created in the test spans, through the centreline of the cross-section, at 138 mm, 413 mm, and 688 mm from the centreline of the support. The vertical holes were created by installing 15 mm diameter acrylic rods at the required positions within the steel reinforcement cage before casting the concrete. The acrylic rods were removed from the concrete two days after casting. For Beams R07 and R12, the vertical holes were blocked by rubber plugs before starting the accelerated corrosion process.

Prior to installing the CFRP rods, the holes were cleaned by a wire brush and compressed air to remove any cement or aggregate residues. The lower ends of the holes were sealed with plastic sheets and a high viscosity epoxy adhesive was used to fill two third of the holes. The CFRP rods were covered with a thin layer of the adhesive and inserted into the holes. Any excess epoxy was removed. The plastic sheets at the lower ends of the holes were removed two days after installing the CFRP rods.

It should be noted that Valerio et al. (2009) demonstrated that it was possible to install the CFRP rods by drilling vertical holes upwards from the soffit. The procedure explained above for installing the CFRP rods was used for simplicity as it did not require drilling holes.

Instrumentation

The load was applied at a displacement-controlled rate of approximately 0.1 mm/min (equivalent to approximately 3 kN/min) using a 500 kN hydraulic jack. Loading was stopped at each 15 kN up to approximately 85% of the estimated failure load in order to record crack propagation.

A comprehensive and carefully planned measuring strategy was implemented. A 250 kN load cell was placed under the support at the end of the test span to measure the actual shear force. The vertical deflection under the applied load was measured using both linear resistance displacement transducers (LRDTs) and dial gauges. Strain gauges (6 mm, 120 Ω) were attached to the shear links in the test spans, CFRP sheets, and embedded CFRP rods as shown in Figure 2.

The readings of the 250 kN load cell, LRDTs, and strain gauges were obtained using a data logger. The readings of the dial gauges were manually recorded.

RESULTS AND DISCUSSION

Accelerated corrosion results

As can be seen in Table 4, the shear links in the test spans of N07, R07, S07, N12, R12, and S12 had average actual corrosion levels of 6.4%, 7.6%, 6.0%, 12.2%, 12.3%, and 12.1% respectively. Except for the shear links in the test span of R07, all the corroded shear links had average actual corrosion levels that are less than the targeted corrosion levels of either 7% or 15%. The average differences between the targeted (based on Faraday's law) and actual (based on gravimetric mass loss) corrosion levels were 11% and 23% for the shear links with nominal corrosion levels of 7% and 15% respectively. Comparable results were reported by Malumbela et al. (2012). El Maaddawy and Soudki (2003) suggested that, at corrosion levels higher than 7%, the amount of corrosion products around the steel reinforcement might hinder the diffusion of the Hydroxide and/or Ferrous ions through the rust layer. This might explain the higher difference between the targeted and actual corrosion levels for the shear links with a nominal corrosion level of 15%.

Table 4 shows that the current density values used in this study had insignificant effect on the average actual corrosion levels. The shear links in the test spans of R12, N12, and S12 were corroded using current density values of 140 μA/cm^2, 185 μA/cm^2, and 200 μA/cm^2 respectively. However, the shear links in the three beams had approximately equal average actual corrosion levels ranging from 12.1% to 12.3%.

Shear strength

Table 5 shows the total shear force attained by each beam at failure. As reported in Table 5, the tested beams had variable cube compressive strengths and therefore it would be inaccurate to directly compare their shear force capacities. In order to reasonably compare the shear strength of the tested beams, the nominal shear stress at failure ($V_{max}/b_w d$) for each beam was divided by the square root of its cube compressive strength, which is a measure of concrete shear strength. The resulting values of normalized shear stress at failure ($V_{max}/b_w d\sqrt{f_{cu}}$) were then divided by the corresponding value for N00 (i.e. 0.76) to calculate the normalized shear stress at failure relative to N00 (see Table 5).

The effect of shear link corrosion level on the shear strength of the unstrengthened beams can be inferred by comparing their normalized shear stresses at failure relative to N00. Increasing the shear link corrosion level decreased the shear strength of N07 and N12 relative to that of N00 by 11% and 14% respectively. As the corrosion level increases, the yield and ultimate stresses and strains of the shear links decrease (Almusallam, 2001) and the bond performance between the shear links and concrete deteriorates. This, in turn, reduces the steel contribution to the shear force capacity which adversely affects the shear strength of the beams.

The shear link nominal corrosion level of 7% did not have a significant effect on the shear strength of the strengthened beams. The difference between the normalized shear stresses at failure for R00 and R07 was about 2%. Similarly, S00 and S07 had a difference of about 4% between their normalized shear stresses at failure. At the actual corrosion level of 12%, the strengthened beams (i.e. R12 and S12) had normalized shear stresses at failure that were approximately 12% less than the corresponding values for the un-corroded beams (i.e. R00 and S00).

As can be seen in Table 5, all strengthened beams had higher normalized shear stresses at failure than the corresponding unstrengthened beams. Of note is that R07 and R12 had normalized shear stresses at failure that were 19% and 12% higher than the corresponding values for N07 and N12 respectively whereas the corresponding percentage enhancements for S07 and S12 were 15% and 11% respectively. The DE technique therefore seems more effective than the EB technique in enhancing the shear strength of RC beams with corroded shear links. The higher effectiveness provided by the DE technique may be explained by two factors. First, the embedded CFRP rods are less susceptible to debonding issues due to the better bond performance between the concrete core and the CFRP reinforcement (Chaallal et al., 2011). Second, the CFRP rods can be embedded along the full effective depth of the beam whereas the presence of the flange limits the effective depth of the EB CFRP sheets.

The effectiveness of both strengthening systems decreased with increasing shear link corrosion level. At the lower shear link corrosion level, the strengthening systems enhanced the normalized shear stresses at failure for R07 and S07 by 7% and 3% respectively relative to that of N00 (i.e. the un-corroded unstrengthened beam). However, at the higher shear link corrosion level, R12 and S12 had normalized shear stresses at failure that were 4% and 5% lower respectively than the corresponding value for N00. Hence, the strengthening systems were almost, but not quite, effective at returning R12 and S12 to their un-corroded shear strength. The reduced effectiveness of the EB technique with increasing shear link corrosion level may be explained by the reduced friction resistance at the shear link/concrete interface which causes early separation of the lateral concrete cover after formation of inclined cracks (El-Maaddawy and Chekfeh, 2013). Further research is required to identify the factors affecting the reduced effectiveness of the DE technique with increasing shear link corrosion level.

Deflection response

Figures 4a-4c show the shear force-deflection curves for the un-corroded, 7% corroded, and 12% corroded beams respectively. All beams featured a quasi-linear shear force-deflection response up to peak shear force. The sudden drop in load at peak shear force is characteristic of brittle (shear) failure. For each beam, the shear force at failure and the corresponding deflection at the loading point are given in Table 5.

Except for the case of the un-corroded beams (Figure 4a), the unstrengthened and DE strengthened beams had comparable stiffness at a given corrosion level whereas the EB beams had a stiffer response. This trend is particularly evident in Figure 4b since N07, R07, and S07 had comparable concrete strengths (see Table 5). Mofidi and Chaallal (2011) suggested that some EB CFRP continuous sheets, although uniaxial, can still carry some load in the direction perpendicular to the fiber orientation. This might explain the higher stiffness of the EB beams compared with those of the unstrengthened and DE strengthened beams.

For the un-corroded beams, R00 had lower concrete strength compared with N00 and S00 (see Table 5). The relatively low concrete tensile strength of R00 (see Table 5) resulted in flexural and shear crack formations at lower shear force values compared with N00 and S00. Crack opening resulted in higher deflections at a given shear force and consequently lower stiffness for R00.

Figure 4d presents the shear force-deflection curves for the beams strengthened with the EB CFRP sheets. These beams had concrete cube compressive strengths ranging from 36.8 MPa to 42.9 MPa. Figure 4d shows that corrosion level had insignificant effect on the deflection response of the EB strengthened beams. Similar results confirming this finding were reported by El-Maaddawy and Chekfeh (2013). Although not detailed in Figure 4 for brevity purposes, the deflection response of both the unstrengthened and the DE strengthened beams was not affected by corrosion level.

Failure mode

The failure modes of the unstrengthened beams are shown in Figure 5. All the unstrengthened beams, regardless of the shear link corrosion level, exhibited a shear mode of failure due to inclined cracks that ran from the support to the load point. In the web, the main inclined cracks followed a path at an angle of approximately 32°, intersecting both the first (i.e. closer to the support) and second (middle) shear links. The inclined cracks followed a much shallower path (approximately 20°) in the flange, intersecting the third (inner) shear link just below the top of the flange. Visual inspection of Beam N12 at failure (see Figure 5) revealed that it had a wider main inclined crack compared with the corresponding cracks in Beams N00 and N07. This was to be expected as the shear links with the 12.2% average corrosion level offered less resistance to crack opening.

Figure 6 shows the failure modes of the beams strengthened with the DE technique. Similar to the unstrengthened beams, R00, R07, and R12 failed in shear due to inclined cracks that extended from the support to the load point. However, the inclined cracks in the beams with embedded CFRP reinforcement were more distributed than the corresponding cracks in the unstrengthened beams. It is well known that increasing the transverse reinforcement ratio in a RC beam results in more distributed and narrower cracks (Zakaria et al., 2009). The crack patterns of R00, R07, and R12 can therefore be attributed to the presence of the embedded CFRP rods. Of note is that there was no sign of debonding between the embedded CFRP rods and the surrounding concrete at failure.

Figure 7 shows the typical failure mode of the beams strengthened with the EB CFRP sheets. Those beams failed due to inclined cracks that penetrated the flange and propagated towards the load point. The crack propagation was accompanied by the debonding of the EB CFRP sheets as depicted in Figure 7. The premature debonding of the EB CFRP sheets may be prevented by anchoring the strengthening system to the concrete using compatible composite anchors. This would increase the effectiveness of the EB CFRP sheets and consequently the shear force carrying capacity of the beams (Eshwar et al. 2008; Mofidi et al. 2012b; Koutas and Triantafillou 2013).

Strain in the shear links and CFRP reinforcement

This section reports on the strain in both the steel shear links and the CFRP strengthening systems. Figure 2 shows the locations of the strain gauges attached to the steel and CFRP shear reinforcement. For the purpose of interpreting results, the shear links and embedded CFRP rods are categorized into outer, middle, and inner shear reinforcement (see Figure 2). Similarly, the strain gauges attached to the EB CFRP sheets are categorized into outer, middle, and inner gauges as depicted in Figure 2. Unfortunately, some strain gauges failed during testing and hence their results were discarded.

Figure 8 shows the shear force-strain variations for the steel shear links. In general, the shear links exhibited two stages of response during loading. In the first stage, the shear links were inactive and therefore did not contribute to the shear force capacity. The second stage is marked by the formation of inclined cracks at a shear force of approximately 50 kN to 75 kN. This variation in inclined cracking shear force is attributable to the variation in concrete tensile strength (see Table 2). After the formation of inclined cracks, the shear links developed strain with increasing shear force until failure occurred.

The outer and middle shear links were more strained compared with the inner shear links. This can be explained by the fact that the outer and middle shear links were intersected by the main shear cracks. The inner shear links were located at a region which did not experience much cracking.

At a given shear link location (i.e. outer, middle, or inner), a shear link in a beam strengthened with the EB CFRP sheets (i.e. S00, S07, or S12) had less strain at a given shear force than the corresponding shear link in a beam strengthened with the DE CFRP rods (i.e. R00, R07, or R12). For example, between a shear force of 65 kN and 140 kN, the strain in the middle shear link in S12 varied between 0.0001 and 0.0010 whereas the strain in the middle shear link in R12 varied between 0.0003 and 0.0020. This result was influenced by two factors. First, the EB CFRP sheets had higher axial rigidity per unit area (1533 MPa) than the DE CFRP rods (283 MPa per rod). Second, the EB CFRP sheets were continuous whereas the DE CFRP rods were located between the shear links (see Figure 2) and therefore could not reduce the strain in the shear links in a similar way to the EB CFRP sheets.

Figure 9(a) shows the shear force-strain variations for the embedded CFRP reinforcement. The behaviour of the embedded CFRP rods was comparable to that of the steel shear links. The shear forces at which the embedded rods started to function were also in the range of 50 kN to 75 kN. For Beam R12, the middle CFRP rod experienced the highest strain at a given shear force as it was intersected by the main shear crack (see Figure 6). At peak shear force, the strain in the embedded CFRP rods was in the range of 0.0013 to 0.0033.

The shear force-strain curves for the EB CFRP sheets are shown in Figure 9(b). The response of the CFRP sheets can be divided into three phases. Initially, the sheets were inactive up to a shear force of approximately 50 kN to 75 kN. At that shear force level, which marks the beginning of the second phase, the sheets started to develop tensile strain as they started to resist crack opening. For a given beam, the regions of the CFRP sheets intersected by the inclined cracks developed strain at a higher rate than the remaining regions of the strengthening system. In the third phase, the fabrics started to debond, as shown by the reversing of the shear force-strain curves in Figure 9(b), and finally peeled off. At peak shear force, debonding limited the highest recorded strain in the CFRP sheets to 0.0013.

CONCLUSIONS

This paper presents the results of an experimental investigation on the structural behavior of un-strengthened as well as CFRP-strengthened RC T-beams with either un-corroded or corroded steel shear links. The tested beams were strengthened with either EB CFRP sheets or embedded CFRP rods. The actual shear link corrosion levels, obtained using gravimetric mass loss, were 0% (un-corroded), 7%, and 12%. Based on the results of this study, the following conclusions are drawn:

1. The unstrengthened beams with shear link corrosion levels of 7% and 12% had shear strengths that were 11% and 14% respectively less than the shear strength of the un-corroded unstrengthened beam.
2. The shear link corrosion level of 7% did not have a significant effect on the shear strength of the strengthened beams. The beams with the shear link corrosion level of 7% and strengthened with the DE or EB CFRP systems had comparable shear strengths to the corresponding un-corroded strengthened beams.
3. At the shear link corrosion level of 12%, the strengthened beams had shear strengths that were approximately 12% less than the corresponding values for the un-corroded strengthened beams. Moreover, the strengthened beams had shear strengths that were approximately 4% to 5% less than the shear strength of the un-corroded

unstrengthened beam. Hence, the strengthening systems were almost, but not quite, effective at returning the beams with the 12% shear link corrosion level to their un-corroded shear strength.

4. The effectiveness of both strengthening systems decreased with increasing shear link corrosion level. The shear strength enhancement provided by the DE and EB CFRP systems decreased from 19% and 15% respectively to 12% and 11% respectively with the increase in shear link corrosion level from 7% to 12%.
5. The corrosion level had insignificant effect on the deflection response of the tested beams.
6. The beams strengthened with the EB technique had stiffer response and less strain in the shear links compared with the corresponding beams strengthened with the DE technique.
7. Debonding resulted in limited strain in the CFRP sheets (less than 0.0013). On the other hand, the embedded CFRP rods did not show signs of debonding and developed higher strains (0.0013 – 0.0043) compared with the EB sheets.

ACKNOWLEDGEMENTS

The authors would like to thank Fyfe Europe for supplying the CFRP sheets and epoxy laminating resin used in this study. The first author acknowledges the financial support of the UK Engineering and Physical Sciences Research Council.

REFERENCES

Almusallam, A.A. (2001). “Effect of degree of corrosion on the properties of reinforcing steel bars.” *Constr. Built. Mater*. 15 (8), 361-368.

ASTM International. (2011). “Standard practice for preparing, cleaning, and evaluating corrosion test specimens.” *ASTM G1-03*, West Conshohocken, PA.

Broomfield, J. P. (2007). “Corrosion of Steel in Concrete: Understanding, Investigation and Repair.” 2nd Edition, Taylor and Francis Group, Oxford, United Kingdom.

Chaallal, O., Mofidi, A., Benmokrane, B., and Neale, K. (2011). “Embedded through-section FRP rod method for shear strengthening of RC Beams: performance and comparison with existing techniques.” *J. Compos. Constr.*, 15(3), 374-383.

Concrete Society. (2009). “Historical approaches to the design of concrete buildings and structures.” *Tech. Rep. No. 70*, Crowthorne, United Kingdom.

Dirar, S., Lees, J., and Morley, C. (2012). “Precracked reinforced concrete T-beams repaired in shear with bonded carbon fiber-reinforced polymer sheets.” *ACI Struct. J.*, 109(2), 215-224.

Dirar, S., Lees, J. M., and Morley, C. T. (2013). “Precracked reinforced concrete T-beams repaired in shear with prestressed carbon-fiber reinforced polymer straps.” *ACI Struct. J.*, 110(5), 855-866.

El-Maaddawy, T., and Chekfeh, Y. (2013). “Shear strengthening of T-Beams with corroded stirrups using composites.” *ACI Struct. J.*, 110(5), 779-790.

El Maaddawy, T., and Soudki, K. (2007). "A model for prediction of time from corrosion initiation to corrosion cracking." *Cement Concrete Comp.*, 29, 168-175.

El-Maaddawy, T. A., and Soudki, K. A. (2003). "Effectiveness of impressed current technique to simulate corrosion of steel reinforcement in concrete." *J. Mater. Civ. Eng.*, 15 (1), 41-47.

Eshwar, N., Nanni, A., and Ibell, T. J. (2008). "Performance of two anchor systems of externally bonded fiber-reinforced polymer laminates." *ACI Mater. J.*, 105(1), 72-80.

Koch, G. H., Brongers, M. P. H., Thompson, N. G., Virmani, Y. P., and Payer, J. H. (2001). "Corrosion cost and preventive strategies in the United States." Report No. FHWA-RD-01-156, Federal Highway Administration, U.S. Department of Transportation, McLean, VA, 82pp.

Koutas, L., and Triantafillou, T. C. (2013). "Use of anchors in shear strengthening of reinforced concrete T-beams with FRP." *J. Compos. Constr.*, 17(1), 101-107.

Malumbela, G., Moyo, P., and Alexander, M. (2012). "A step towards standardising accelerated corrosion tests on laboratory reinforced concrete specimens." *J. S. Afr. Inst. Civ. Eng.*, 54(2), 78-85.

Mofidi, A., and Chaallal, O. (2011). "Shear strengthening of RC beams with externally bonded FRP composites: Effect of strip-width-to-strip-spacing ratio." J. Compos. Constr., 15(5), 732-742.

Mofidi, A., Chaallal, O., Benmokrane, B., and Neale, K. (2012a). "Experimental tests and design model for RC beams strengthened in shear using the embedded through-section FRP method." *J. Compos. Constr.*, 16(5), 540-550.

Mofidi, A., Chaallal, O., Benmokrane, B., and Neale, K. (2012b). "Performance of end-anchorage systems for RC beams strengthened in shear with epoxy-bonded FRP." *J. Compos. Constr.*, 16(3), 322-331.

Mofidi, A., Thivierge, S., Chaallal, O., and Shao, Y. (2014). "Behavior of reinforced concrete beams strengthened in shear using L-shaped CFRP plates: experimental investigation." *J. Compos. Constr.*, 10.1061/(ASCE)CC.1943-5614.0000398, 04013033.

Rahal, K. N., and Rumaih, H. A. (2011). "Tests on reinforced concrete beams strengthened in shear using near surface mounted CFRP and steel bars." *Eng. Struct.,* 33(1), 53-62.

Valerio, P., and Ibell, T. J. (2003). "Shear strengthening of existing concrete bridges." *Struct. Build.*, 156, 75-84.

Valerio, P., Ibell, T. J., and Darby, A. P. (2009). "Deep embedment of FRP for concrete shear strengthening." *Struct. Build.*, 162, 311-321.

Xia, J., Jin, W. L., and Li, L. Y. (2011). "Shear performance of reinforced concrete beams with corroded stirrups in chloride environment." *Corros. Sci.*, 53(5), 1794-1805.

Zakaria, M., Ueda, T., Wu, Z., and Meng, L. (2009). "Experimental investigation on shear cracking behavior in reinforced concrete beams with shear reinforcement." *J. Adv. Concr. Technol.*, 7(1), 79-96.

LIST OF TABLES

Table 1 Test specimens

Table 2 Concrete properties

Table 3 Steel reinforcement properties

Table 4 Corrosion level results

Table 5 Test results

Table 1 Test specimens

Group	Beam designation	Time of exposure to corrosion (sec)	Applied current density ($\mu A/cm^2$)	Targeted corrosion level (%)	Strengthening scheme
N	N00	-	-	-	All beams in Group N were unstrengthened
	N07	2006880	200	7	
	N12	4579200	185	15	
R	R00	-	-	-	10 mm CFRP rods @ 275 mm spacing
	R07	1995180	200	7	
	R12	6065940	140	15	
S	S00	-	-	-	One layer of continuous EB CFRP sheets
	S07	1998120	200	7	
	S12	4251600	200	15	

Table 2 Concrete properties

Beam designation	Cube compressive strength (MPa)		Cylinder split tensile strength (MPa)		Flexural strength (MPa)	
	Average(1)	Standard deviation(1)	Average(2)	Standard deviation(2)	Average(2)	Standard deviation(2)
N00	26.3	2.4	2.3	0.7	4.1	0.2
N07	35.1	1.0	2.6	0.2	5.4	0.4
N12	41.8	2.1	2.2	0.1	6.1	0.4
R00	21.7	1.3	1.5	0.2	3.1	0.2
R07	37.0	1.0	2.0	0.4	5.1	0.2
R12	37.0	1.3	1.9	0.1	5.3	0.4
S00	37.0	1.4	2.4	0	4.2	0.7
S07	36.8	0.9	2.5	0.3	5.4	0.5
S12	42.9	1.3	2.1	0.4	6.1	0.3

(1) Based on at least five samples per beam
(2) Based on three samples per beam

Table 3 Steel reinforcement properties

Bar diameter (mm)	Yield strength (MPa)	Yield strain (mm/mm)	Ultimate strength (MPa)	Elastic modulus (GPa)
8 (test span)	542	0.003	664	186
8 (non-test span)	573	0.003	655	183
20	576	0.003	707	179
25	537	0.003	669	180

Table 4 Corrosion level results

Shear link designation	Original mass (g)	Applied current (mA)	Applied current density (μA/cm^2)	Residual mass (g)	Theoretical corrosion level (%)	Actual corrosion level (%)	Average actual corrosion level (%)
N07/1st	688	89.6	200	641	7.6	6.8	
N07/2nd	687	89.6	200	646	7.6	6.0	6.4
N07/3rd	683	89.2	200	640	7.6	6.3	
R07/1st	684	89.4	200	634	7.5	7.3	
R07/2nd	693	90.5	200	642	7.5	7.4	7.6
R07/3rd	688	89.9	200	633	7.5	8.0	
S07/1st	686	89.3	200	640	7.5	6.7	
S07/2nd	690	89.8	200	651	7.5	5.7	6.0
S07/3rd	691	90.0	200	652	7.5	5.6	
N12/1st	690	83.3	185	609	16.0	11.7	
N12/2nd	689	83.3	185	611	16.0	11.3	12.2
N12/3rd	700	83.3	185	605	15.8	13.6	
R12/1st	688	189*	140	612	15.9	11.0	
R12/2nd	699	189*	140	614	15.9	12.2	12.3
R12/3rd	692	189*	140	598	15.9	13.6	
S12/1st	699	91.2	200	615	16.1	12.0	
S12/2nd	686	89.3	200	614	16.0	10.5	12.1
S12/3rd	687	89.5	200	592	16.0	13.8	

* Connected in series

Table 5 Test results

Beam designation	Average cube compressive strength (MPa)	Total shear force (kN)	Normalized shear stress at failure	Normalized shear stress at failure relative to N00	Deflection at loading point (mm)	Failure mode
N00	26.3	143	0.76	1.00	7.39	Shear
N07	35.1	148	0.68	0.89	8.73	Shear
N12	41.8	155	0.65	0.86	9.29	Shear
R00	21.7	142	0.83	1.09	9.57	Shear
R07	37.0	182	0.81	1.07	10.54	Shear
R12	37.0	164	0.73	0.96	9.69	Shear
S00	37.0	182	0.81	1.07	9.02	Shear
S07	36.8	174	0.78	1.03	7.62	Shear
S12	42.9	174	0.72	0.95	9.24	Shear

LIST OF FIGURES

Figure 1 Cross-sections – all dimensions in mm

Figure 2 Test setup: (a) unstrengthened beams, (b) DE CFRP strengthened beams, and (c) EB CFRP strengthened beams – all dimensions in mm

Figure 3 Accelerated corrosion setup

Figure 4 Shear force-deflection curves: (a) un-corroded beams, (b) 7% corroded beams, (c) 12% corroded beams, and (d) EB strengthened beams

Figure 5 Unstrengthened beams at failure

Figure 6 Beams strengthened with the embedded CFRP rods at failure

Figure 7 Typical failure mode of the beams strengthened with the EB CFRP sheets

Figure 8 Shear force-strain curves: (a) outer shear links, (b) middle shear links, and (c) inner shear links

Figure 9 Shear force-strain curves: (a) CFRP rods and (b) CFRP sheets

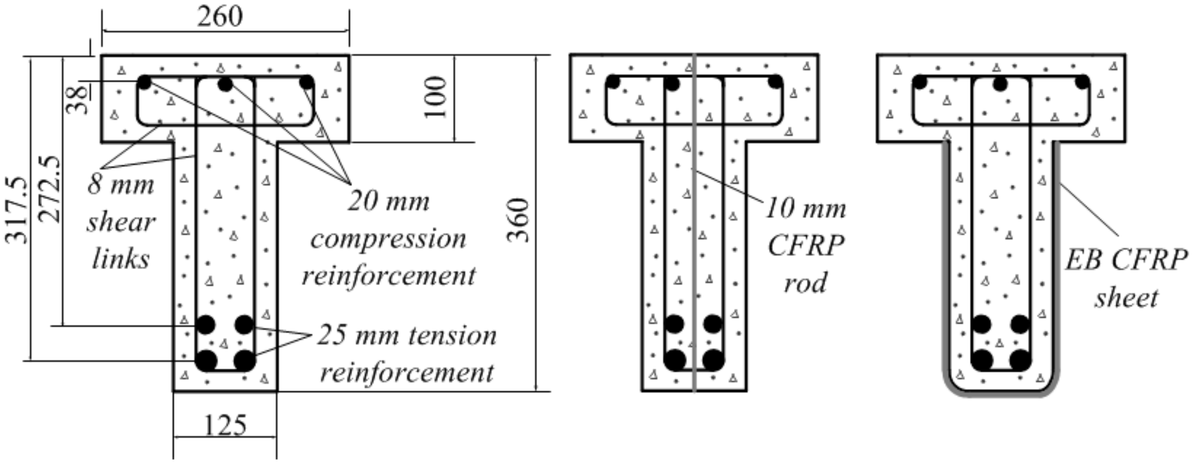

Figure 1 Cross-sections – all dimensions in mm

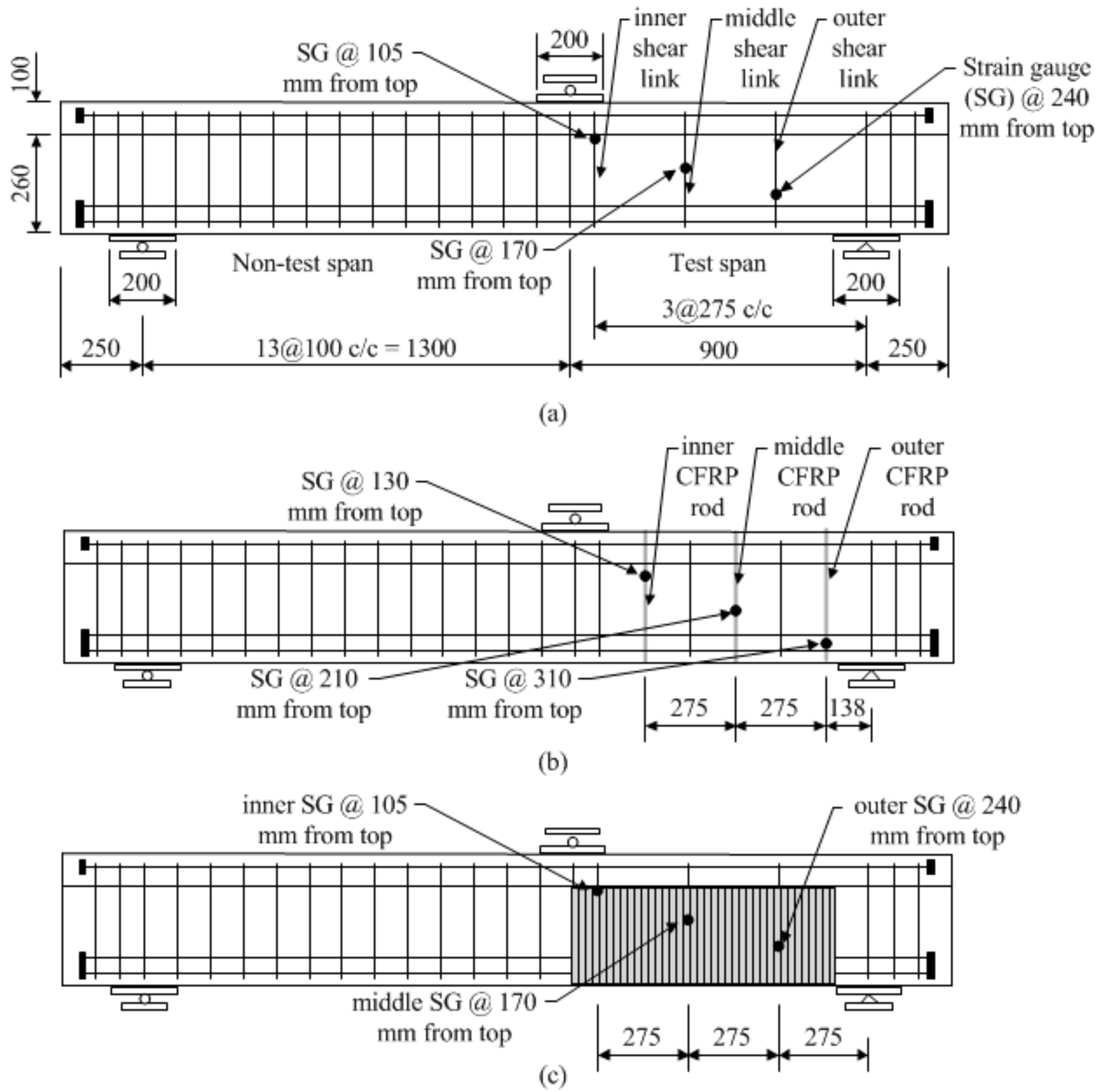

Figure 2 Test setup: (a) unstrengthened beams, (b) DE CFRP strengthened beams, and (c) EB CFRP strengthened beams – all dimensions in mm

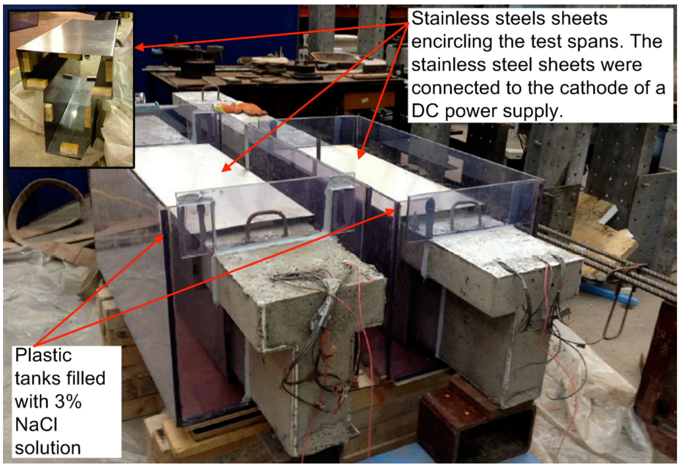

Figure 3 Accelerated corrosion setup

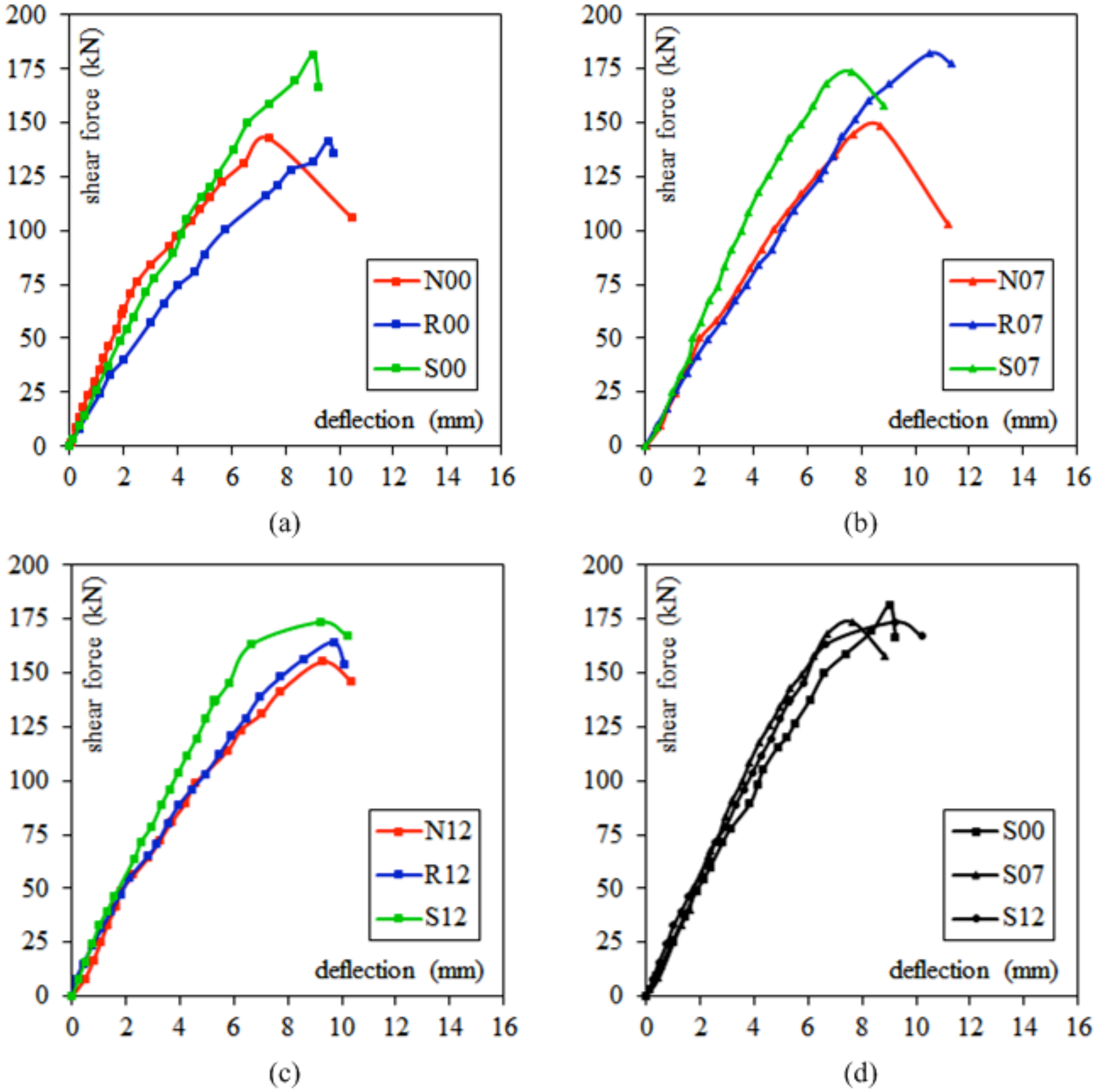

Figure 4 Shear force-deflection curves: (a) un-corroded beams, (b) 7% corroded beams, (c) 12% corroded beams, and (d) EB strengthened beams

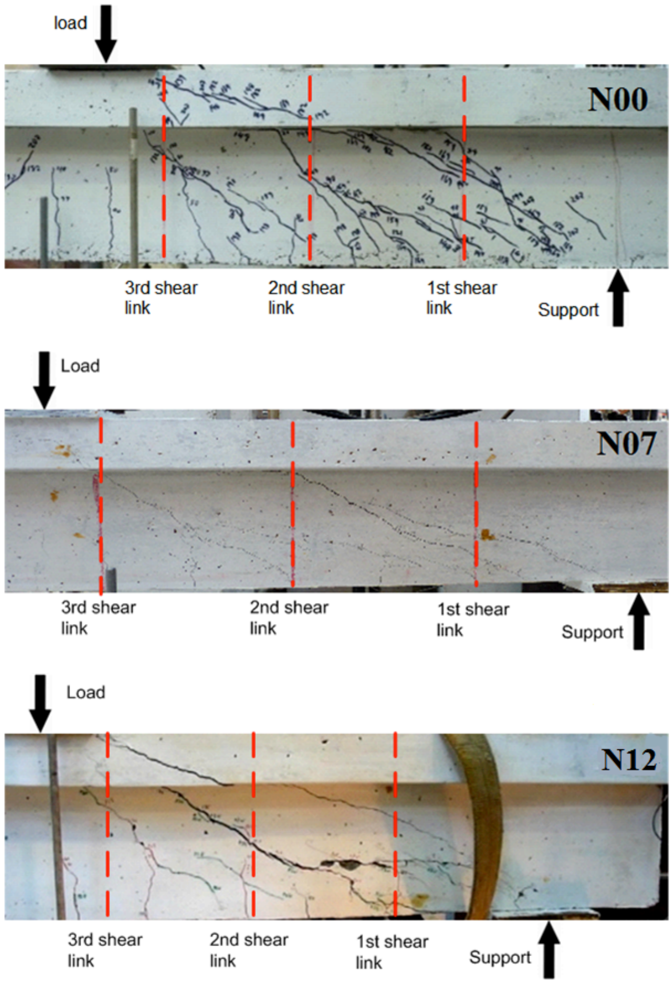

Figure 5 Unstrengthened beams at failure

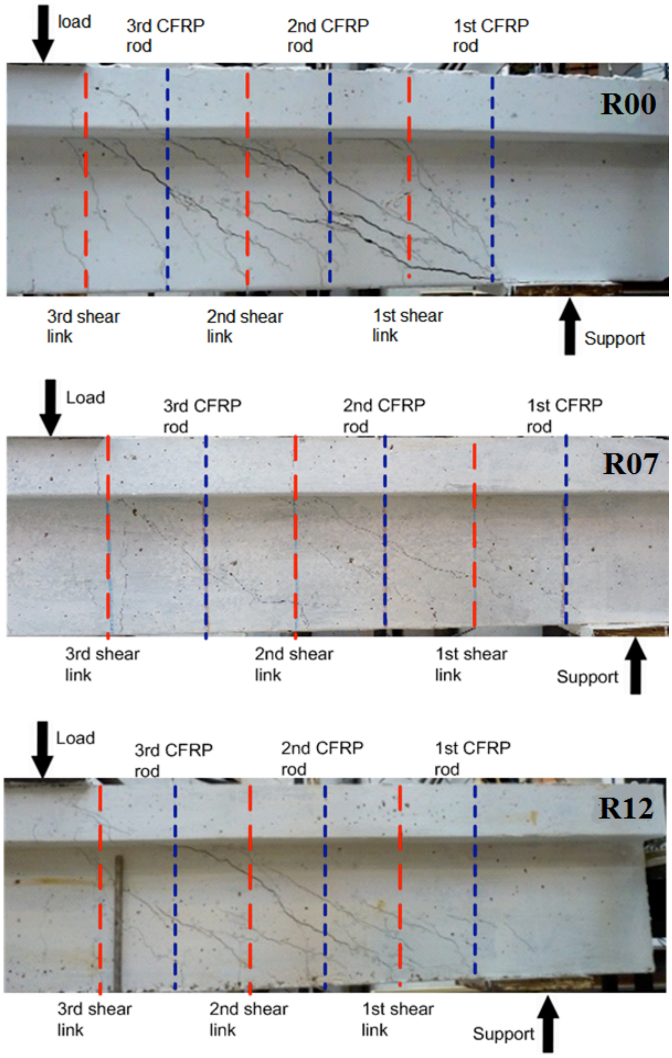

Figure 6 Beams strengthened with the embedded CFRP rods at failure

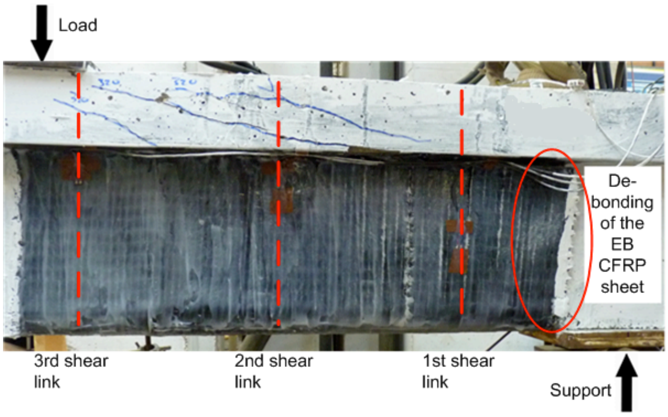

Figure 7 Typical failure mode of the beams strengthened with the EB CFRP sheets

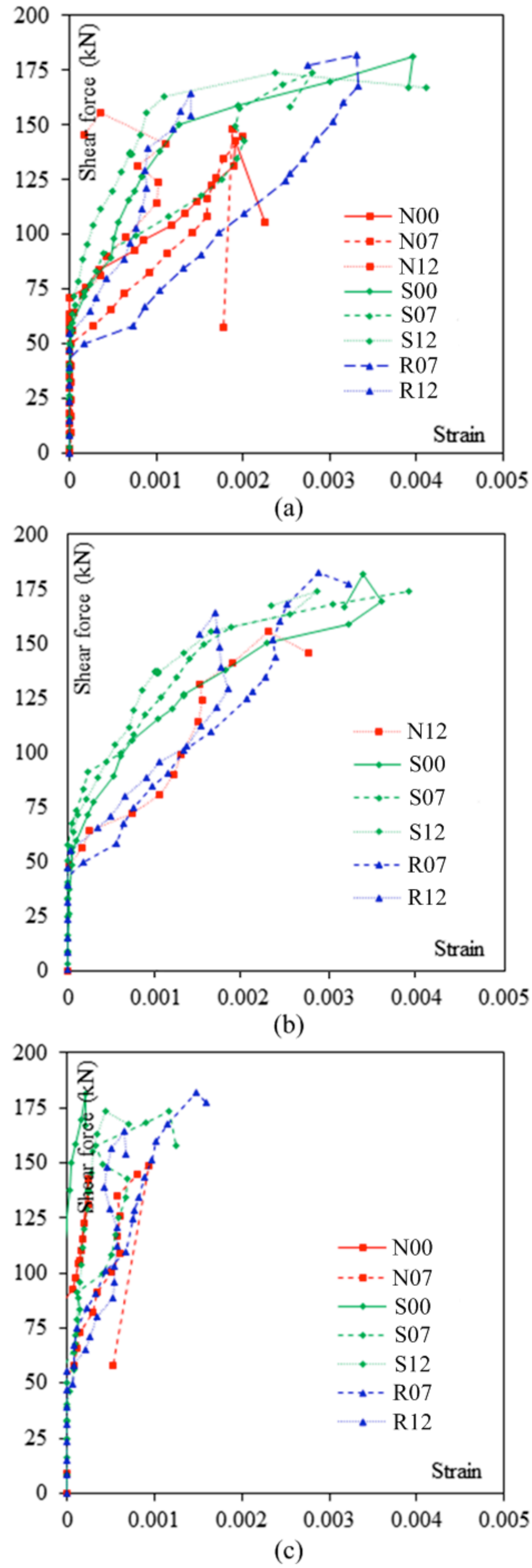

Figure 8 Shear force-strain curves: (a) outer shear links, (b) middle shear links, and (c) inner shear links

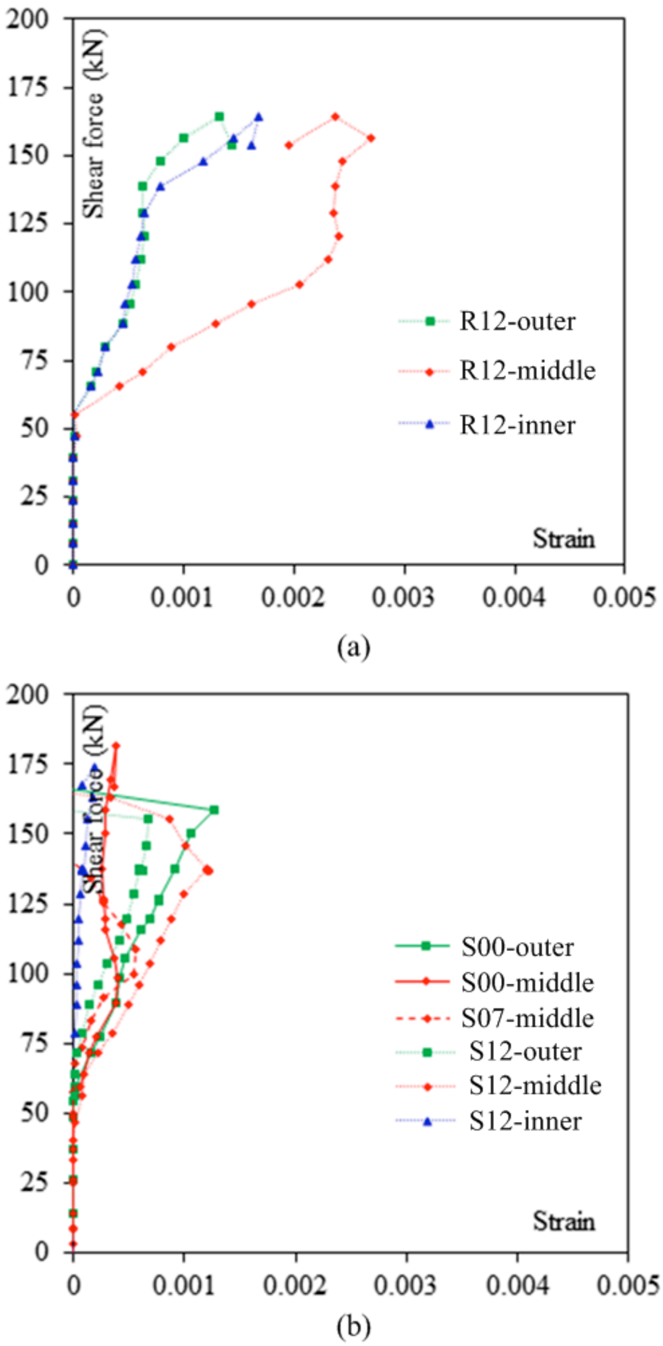

Figure 9 Shear force-strain curves: (a) CFRP rods and (b) CFRP sheets